State-dependent forces in cold quantum gases

Christopher Billington

Submitted in total fulfilment of the requirements
of the degree of Doctor of Philosophy

Supervisory committee:
Prof Kristian Helmerson
Dr Lincoln Turner
Dr Russell Anderson

School of Physics and Astronomy
Monash University

August, 2016

rev: 15 (206c9c70753a)
author: Chris Billington <chrisjbillington@gmail.com>
date: Sun Jul 24 16:55:15 2016 +1000
summary: Draft plots added to hidden variables section.

Blank page after contents page added.

This page intentionally left blank

Contents


```
rev:     15 (206c9c70753a)
author:  Chris Billington <chrisjbillington@gmail.com>
date:    Sun Jul 24 16:55:15 2016 +1000
summary: Draft plots added to hidden variables section.

Blank page after contents page added.
```

This page intentionally left blank

Chapter 3

Quantum mechanics on a computer

3.6 Fourth order Runge–Kutta in an instantaneous local interaction picture

Consider the differential equation for the components of a state vector $|\psi(t)\rangle$ in a particular basis with basis vectors $|n\rangle$. This might simply be the Schrödinger equation, or perhaps some sort of nonlinear or other approximate, effective or phenomenological equation not corresponding to pure Hamiltonian evolution. Though they may have additional terms, such equations are generally of the form:

$$\frac{\mathrm{d}}{\mathrm{d}t}\langle n|\psi(t)\rangle = -\frac{i}{\hbar}\sum_m \langle n|\hat{H}(t)|m\rangle\,\langle m|\psi(t)\rangle\,, \tag{3.1}$$

where $\langle n|\hat{H}(t)|m\rangle$ are the matrix elements in that basis of the Hamiltonian $\hat{H}(t)$, which in general can be time dependent, or even a function of $|\psi(t)\rangle$, depending on the exact type of equation in use. If $\hat{H}(t)$ is almost diagonal in the $|n\rangle$ basis, then the solution to (3.1) is dominated by simple dynamical phase evolution, that is:

$$|\psi(t)\rangle \approx \sum_m e^{-\frac{i}{\hbar}E_m t}\,|m\rangle\,, \tag{3.2}$$

where E_m is the energy eigenvalue corresponding to the eigenstate $|m\rangle$.

A transformation into an interaction picture (IP) [1, p318] is commonly used to treat this part of the evolution analytically, before solving the remaining dynamics with further analytics or numerics. For numerical methods, integration in the interaction picture allows one to use larger integration timesteps, as one does not need to resolve the fast oscillations around the complex plane due to this dynamical phase.

Choosing an interaction picture typically involves diagonalising the time-independent part of a Hamiltonian, and then proceeding in the basis in which that time-independent part is diagonal. However, often one has a good reason to perform computations in a different basis, in which the time independent part of the Hamiltonian is only approximately diagonal,[1] and transforming between bases may be computationally expensive (involving large matrix-vector multiplications). Furthermore, the Hamiltonian may change sufficiently during the time interval being simulated that the original time-independent Hamiltonian no longer dominates the dynamics at later times. In both these cases it would still be useful to factor out the time-local oscillatory dynamics in whichever basis is being used, in order to avoid taking unreasonably small timesteps.

[1] For example, a spatial basis which allows for partitioning the integration region over multiple nodes on a cluster or cores on a GPU.

To that end, suppose we decompose $\hat{H}(t)$ into diagonal and non-diagonal (in the $|n\rangle$ basis) parts at each moment in time:

$$\hat{H}(t) = \hat{H}_{\text{diag}}(t) + \hat{H}_{\text{nondiag}}(t), \tag{3.3}$$

```
rev:     15 (206c9c70753a)
author:  Chris Billington <chrisjbillington@gmail.com>
date:    Sun Jul 24 16:55:15 2016 +1000
summary: Draft plots added to hidden variables section.

Blank page after contents page added.
```

and use the diagonal part at a specific time $t = t'$ to define a time-independent Hamiltonian:

$$\hat{H}_0^{t'} = \hat{H}_{\text{diag}}(t'), \tag{3.4}$$

which is diagonal in the $|n\rangle$ basis. We can then use then use $\hat{H}_0^{t'}$ to define an interaction picture state vector:

$$|\psi_{\text{I}}^{t'}(t)\rangle = e^{\frac{i}{\hbar}(t-t')\hat{H}_0^{t'}} |\psi(t)\rangle\,, \tag{3.5}$$

which obeys the differential equation:

$$\frac{\mathrm{d}}{\mathrm{d}t}|\psi_{\text{I}}^{t'}(t)\rangle = e^{\frac{i}{\hbar}(t-t')\hat{H}_0^{t'}} \frac{\mathrm{d}}{\mathrm{d}t}|\psi(t)\rangle + \frac{i}{\hbar}\hat{H}_0^{t'}|\psi_{\text{I}}^{t'}(t)\rangle\,, \tag{3.6}$$

where:

$$|\psi(t)\rangle = e^{-\frac{i}{\hbar}(t-t')\hat{H}_0^{t'}} |\psi_{\text{I}}^{t'}(t)\rangle \tag{3.7}$$

is the original Schrödinger picture (SP) state vector.

This transformation is exact, no approximations or assumptions have been made. If indeed the dynamics of $|\psi(t)\rangle$ in the given basis are dominated by fast oscillating dynamical phases, that is, the diagonals of $\hat{H}_{\text{diag}}(t)$ are much greater than all matrix elements of $\hat{H}_{\text{nondiag}}(t)$ in the $|n\rangle$ basis, then solving the differential equation (3.6) for $|\psi_{\text{I}}^{t'}(t)\rangle$ should allow one to use larger integration timesteps than solving (3.1) directly. And if not, then it should do no harm other than the (small) computational costs of computing some extra scalar exponentials.

Equation (3.5) defines an *instantaneous* interaction picture, in that it depends on the dynamics at a specific time $t = t'$, and can be recomputed repeatedly throughout a computation in order to factor out the fast dynamical phase evolution even as the oscillation rates change over time. It is *local* in that $H_0^{t'}$ is diagonal in the $|n\rangle$ basis, which means that transformations between Schrödinger picture and interaction picture state vectors involves ordinary, elementwise exponentiation of vectors, rather than matrix products. Thus (3.5), (3.6) and (3.7) can be written componentwise as:

$$\langle n|\psi_{\text{I}}^{t'}(t)\rangle = e^{i(t-t')\omega_n^{t'}} \langle n|\psi(t)\rangle\,, \tag{3.8}$$

$$\frac{\mathrm{d}}{\mathrm{d}t}\langle n|\psi_{\text{I}}^{t'}(t)\rangle = e^{i(t-t')\omega_n^{t'}} \frac{\mathrm{d}}{\mathrm{d}t}\langle n|\psi(t)\rangle + i\omega_n^{t'}\langle n|\psi_{\text{I}}^{t'}(t)\rangle\,, \tag{3.9}$$

and:

$$\langle n|\psi(t)\rangle = e^{-i(t-t')\omega_n^{t'}} \langle n|\psi_{\text{I}}^{t'}(t)\rangle\,, \tag{3.10}$$

where we have defined:

$$\omega_n^{t'} = \frac{1}{\hbar}\langle n|\hat{H}_0^{t'}|n\rangle \tag{3.11}$$

This is in contrast to fourth order Runge–Kutta in the interaction picture (RK4IP) [2], in which the interaction picture uses the Fourier basis and thus transforming to and from it involves fast Fourier transforms (FFTs). RK4IP was developed to augment computations in which FFTs were already in use for evaluating spatial derivatives, and so its use of FFTs imposes no additional cost. Nonetheless, an interaction picture based on the kinetic term of the Schrödinger equation (which is the term of the Hamiltonian that RK4IP takes as its time-independent part) may not be useful if that term does not dominate the Hamiltonian, as in the case of a Bose–Einstein condensate in the Thomas–Fermi limit. We compare the two methods below.

```
rev:     15 (206c9c70753a)
author:  Chris Billington <chrisjbillington@gmail.com>
date:    Sun Jul 24 16:55:15 2016 +1000
summary: Draft plots added to hidden variables section.

Blank page after contents page added.
```

3.6.1 Algorithm

The *fourth order Runge–Kutta in an instantaneous local interaction picture* RK4ILIP algorithm is now obtained by using (3.5) to define a new interaction picture at the beginning of each fourth-order Runge–Kutta (RK4) integration timestep. The differential equation and initial conditions supplied to the algorithm are in the ordinary Schrödinger picture, and the interaction picture is used only within a timestep, with the Schrödinger picture state vector returned at the end of each timestep. Thus differential equations need not be modified compared to if ordinary RK4 were being used, and the only modification to calling code required is for a function to compute and return $\omega_n^{t'}$.

Being based on fourth order Runge–Kutta integration, this new method enjoys all the benefits of a workhorse method that is time-proven, and—as evidenced by its extremely widespread use—at a sweet-spot of ease of implementation, accuracy, and required computing power [3].

Below is the resulting algorithm for performing one integration timestep. It takes as input the time t_0 at the start of the timestep, the timestep size Δt, an array $\boldsymbol{\psi}_0$ containing the components $\{\langle n|\psi(t_0)\rangle\}$ of the state vector at time t_0, a function $F(t, \boldsymbol{\psi})$ which takes a time and (the components of) a state vector and returns an array containing the time derivative of each component, and a function $G(t, \boldsymbol{\psi})$ which takes the same inputs and returns an array containing the interaction picture oscillation frequency ω_n for each component at that time.

For example, for the case of the Gross–Pitaevskii equation [4] in the spatial basis $\psi(\boldsymbol{r}, t) = \langle \boldsymbol{r}|\psi(t)\rangle$, these would be:

$$F(t, \psi(\boldsymbol{r}, t)) = -\frac{i}{\hbar}\Big[\underbrace{-\frac{\hbar^2}{2m}\nabla^2}_{\hat{H}_{\text{nondiag}}} + \underbrace{V(\boldsymbol{r}, t) + g|\psi(\boldsymbol{r}, t)|^2}_{\hat{H}_{\text{diag}}}\Big]\psi(\boldsymbol{r}, t), \tag{3.12}$$

and

$$G(t, \psi(\boldsymbol{r}, t)) = \frac{1}{\hbar}\Big[\underbrace{V(\boldsymbol{r}, t) + g|\psi(\boldsymbol{r}, t)|^2}_{\hat{H}_{\text{diag}}}\Big]. \tag{3.13}$$

Note that each symbol in bold in the algorithm below denotes an array containing one element for each basis vector $|n\rangle$, subscripts denote the different stages of RK4, and all arithmetic operations between arrays are elementwise[2] The only opportunity for non-elementwise operations to occur is within F, which contains the details (via $\hat{H}_{\text{nondiag}}$) of any couplings between basis states for whatever system of equations is being solved, for example, using FFTs or finite differences to evaluate the Laplacian in (3.12).

[2] For example, the expression $\boldsymbol{a} \leftarrow e^{-i\boldsymbol{\omega}\Delta t}\boldsymbol{b}$ indicates that for all n, $a_n \leftarrow e^{-i\omega_n \Delta t} b_n$, where a_n denotes the n^{th} element of $\boldsymbol{a}$ etc.

Algorithm 1 RK4ILIP

function RK4ILIP(t_0, Δt, $\boldsymbol{\psi}_0$, F)

$\boldsymbol{f}_1 \leftarrow F(t_0, \boldsymbol{\psi}_0)$ ▷ First evaluation of Schrödinger picture DE

$\boldsymbol{\omega} \leftarrow G(t_0, \boldsymbol{\psi}_0)$ ▷ Oscillation frequencies: $\hbar\omega_n = \langle n|\hat{H}_{\text{diag}}(t_0)|n\rangle$

$\boldsymbol{k}_1 \leftarrow \boldsymbol{f}_1 + i\boldsymbol{\omega}\boldsymbol{\psi}_0$ ▷ Evaluate (3.9) with $t - t' = 0$

$\boldsymbol{\phi}_1 \leftarrow \boldsymbol{\psi}_0 + \boldsymbol{k}_1 \frac{\Delta t}{2}$ ▷ First RK4 estimate of IP state vector, at $t = t_0 + \frac{\Delta t}{2}$

$\boldsymbol{\psi}_1 \leftarrow e^{-i\boldsymbol{\omega}\frac{\Delta t}{2}}\boldsymbol{\phi}_1$ ▷ Convert first estimate back to SP with (3.10)

$\boldsymbol{f}_2 \leftarrow F(t_0 + \frac{\Delta t}{2}, \boldsymbol{\psi}_1)$ ▷ Second evaluation of Schrödinger picture DE

$\boldsymbol{k}_2 \leftarrow e^{i\boldsymbol{\omega}\frac{\Delta t}{2}}\boldsymbol{f}_2 + i\boldsymbol{\omega}\boldsymbol{\phi}_1$ ▷ Evaluate (3.9) with $t - t' = \frac{\Delta t}{2}$

$\boldsymbol{\phi}_2 \leftarrow \boldsymbol{\psi}_0 + \boldsymbol{k}_2 \frac{\Delta t}{2}$ ▷ Second RK4 estimate of IP state vector, at $t = t_0 + \frac{\Delta t}{2}$

$\boldsymbol{\psi}_2 \leftarrow e^{-i\boldsymbol{\omega}\frac{\Delta t}{2}}\boldsymbol{\phi}_2$ ▷ Convert second estimate back to SP with (3.10)

```
rev:     15 (206c9c70753a)
author:  Chris Billington <chrisjbillington@gmail.com>
date:    Sun Jul 24 16:55:15 2016 +1000
summary: Draft plots added to hidden variables section.

Blank page after contents page added.
```

11: $\boldsymbol{f}_3 \leftarrow F(t_0 + \frac{\Delta t}{2}, \boldsymbol{\psi}_2)$ ▷ Third evaluation of Schrödinger picture DE
12: $\boldsymbol{k}_3 \leftarrow e^{i\boldsymbol{\omega}\frac{\Delta t}{2}}\boldsymbol{f}_3 + i\boldsymbol{\omega}\boldsymbol{\phi}_2$ ▷ Evaluate (3.9) with $t - t' = \frac{\Delta t}{2}$
13: $\boldsymbol{\phi}_3 \leftarrow \boldsymbol{\psi}_0 + \boldsymbol{k}_3\Delta t$ ▷ Third RK4 estimate of IP state vector, at $t = t_0 + \Delta t$
14: $\boldsymbol{\psi}_3 \leftarrow e^{-i\boldsymbol{\omega}\Delta t}\boldsymbol{\phi}_3$ ▷ Convert third estimate back to SP with (3.10)
15: $\boldsymbol{f}_4 \leftarrow F(t_0 + \Delta t, \boldsymbol{\psi}_3)$ ▷ Fourth evaluation of Schrödinger picture DE
16: $\boldsymbol{k}_4 \leftarrow e^{i\boldsymbol{\omega}\Delta t}\boldsymbol{f}_4 + i\boldsymbol{\omega}\boldsymbol{\phi}_3$ ▷ Evaluate (3.9) with $t - t' = \Delta t$
17: $\boldsymbol{\phi}_4 \leftarrow \boldsymbol{\psi}_0 + \frac{\Delta t}{6}(\boldsymbol{k}_1 + 2\boldsymbol{k}_2 + 2\boldsymbol{k}_3 + \boldsymbol{k}_4)$ ▷ Fourth RK4 estimate, at $t = t_0 + \Delta t$
18: $\boldsymbol{\psi}_4 \leftarrow e^{-i\boldsymbol{\omega}\Delta t}\boldsymbol{\phi}_4$ ▷ Convert fourth estimate back to SP with (3.10)
19: **return** $\boldsymbol{\psi}_4$ ▷ Return the computed SP state vector at $t = t_0 + \Delta t$
20: **end function**

Note on imaginary time evolution

When RK4ILIP is used for imaginary time evolution (ITE) [5], the oscillation frequencies $\boldsymbol{\omega}$ may have a large imaginary part. If the initial guess is different enough from the ground state, then the exponentials in (3.8), (3.9) and (3.10) may result in numerical overflow. To prevent this, one can define a clipped copy of $\boldsymbol{\omega}$,

$$\boldsymbol{\omega}_{\text{clipped}} = \text{Re}(\boldsymbol{\omega}) + i\begin{cases} -\frac{\log X}{\Delta t} & \text{Im}(\boldsymbol{\omega})\Delta t < -\log X \\ \text{Im}(\boldsymbol{\omega}) & -\log X \leq \text{Im}(\boldsymbol{\omega})\Delta t \leq \log X \\ \frac{\log X}{\Delta t} & \text{Im}(\boldsymbol{\omega})\Delta t > \log X \end{cases}, \tag{3.14}$$

where X is very large but less than the largest representable floating-point number, and use $\boldsymbol{\omega}_{\text{clipped}}$ in the exponents instead. In the below results I used RK4ILIP with ITE to smooth initial states of a Bose–Einstein condensate after a phase printing, and performed clipping with [3] $\log X = 400$.

This clipped version of $\boldsymbol{\omega}$ should be used in all exponents in the above algorithm, but only in exponents—not in the second term of (3.9). If it is used everywhere then all we have done is chosen a different (less useful) interaction picture, and the algorithm will still overflow. By clipping only the exponents, we produce temporarily "incorrect" evolution[4], limiting the change in magnitude of each component of the state vector to a factor of X per step (remembering that X is very large). This continues for the few steps that it takes ITE to get all components of the state vector to within a factor of X of the ground state, after which no clipping is necessary and convergence to the ground state proceeds as normal, subject to the ordinary limitations on which timesteps may be used with ITE.

[3] 400 being about half the largest (base e) exponent representable in double-precision floating point.

[4] Of no concern since we are using ITE as a relaxation method, and are not interested in intermediate states. Only the final state's correctness concerns us.

3.6.2 Domain of improvement over other methods

For simulations in the spatial basis, RK4ILIP treats the spatially local part of the Hamiltonian analytically to first order, and hence can handle larger potentials than ordinary RK4. However, since a global energy offset can be applied to any potential with no physically meaningful change in the results, ordinary RK4 can also handle large potentials — if they are large due a a large constant term which can simply be subtracted off.

So RK4ILIP is only of benefit in the case of large *spatial variations* in the potential. Only one constant can be subtracted off potentials without changing the physics — subtracting a spatially varying potential would require modification of the differential equation in the manner of a gauge transformation in order to leave the system physically unchanged[5].

However that's not quite all: large spatial variation in potentials often comes with the prospect of the potential energy turning into kinetic energy, in which case RK4ILIP is

[5] Though a numerical solution based on analytically gauging away potentials at each timestep might be equally as fruitful as RK4ILIP.

```
rev:     15 (206c9c70753a)
author:  Chris Billington <chrisjbillington@gmail.com>
date:    Sun Jul 24 16:55:15 2016 +1000
summary: Draft plots added to hidden variables section.

Blank page after contents page added.
```

Method	RK4	RK4IP	RK4ILIP	FSS
Error	$\mathcal{O}(\Delta t^4)$	$\mathcal{O}(\Delta t^4)$	$\mathcal{O}(\Delta t^4)$	$\mathcal{O}(\Delta t^2)$
FFTs per step	4	4	4	2
Large ΔV	No	No	Yes	Yes
Large kinetic term	No	Yes	No	Yes
Arbitrary operators	Yes	Yes†	Yes	No
Locally parallelisable	Yes	No	Yes	No
Arbitrary boundary conditions	Yes	No	Yes	No

Table 3.1: Advantages and disadvantages of four timestepping methods for simulating Bose–Einstein condensates. *Large* ΔV refers to whether the method can simulate potentials that vary throughout space by an amount larger than the energy scale $2\pi\hbar/\Delta t$ associated with the simulation timestep Δt. *Arbitrary operators* refers to whether the method permits operators that are not diagonal in either the spatial or Fourier basis, such as angular momentum operators. *Locally parallelisable* means the method can be formulated so as to use only spatially nearby points in evaluating operators, and thus is amenable to parallelisation by splitting the simulation over multiple cores in the spatial basis. † Whilst one can include arbitrary operators within the RK4IP method, only operators diagonal in Fourier space can be analytically treated the way RK4IP treats the kinetic term, and so there is no advantage for these terms over ordinary RK4.

also of little benefit, since in order to resolve the dynamical phase due to the large kinetic term, it would require timesteps just as small as those which ordinary RK4 would need to resolve the dynamical phase evolution from the large potential term.

This leaves RK4ILIP with an advantage only in the case of large spatial variations in the potential that do not lead to equally large kinetic energies. Hence the examples I show in the next section are ones in which the condensate is trapped in a steep potential well—the trap walls are high and hence involve large potentials compared to the interior, but do not lead to large kinetic energies because the condensate is trapped close to its ground state.

The Fourier split-step (FSS) method [6] (see section [TODO]) also models dynamical phases due to the potential analytically to low order. As such it is also quite capable of modeling large potentials. However, it requires that all operators be diagonal in either the spatial basis or the Fourier basis [6]. Therefore BECs in rotating frames, due to the Hamiltonian containing an angular momentum operator, are not amenable to simulation with FSS[6].

This use of FFTs in both the FSS and RK4IP methods necessarily imposes periodic boundary conditions on a simulation, which may not be desirable. By contrast, if different boundary conditions are desired, finite differences instead of FFTs can be used to evaluate spatial derivatives in the RK4 and RK4ILIP methods, so long as a sufficiently high-order finite difference scheme is used so as not to unacceptably impact accuracy.

Along with the ability to impose arbitrary boundary conditions, finite differences require only local data, that is, only points spatially close to the point being considered need be known in order to evaluate derivatives there. This makes finite differences amenable to simulation on cluster computers [8, p100], with only a small number of points (depending on the order of the scheme) needing to be exchanged at node-boundaries each step. By contrast, FFT based derivatives require data from the entire spatial region. Whilst this can still be parallelised on a GPU, where all the data is available, it cannot be done on a cluster without large amounts of data transfer between nodes [9]. Thus, RK4 and RK4ILIP, being implementable with finite difference schemes, are considerably friendlier to cluster computing.

Table3.1 summarises the capabilities of the four methods considered in the following results section. RK4ILIP is the only method capable of modelling a large spatial variation in the potential term whilst being locally parallelisable, and supporting arbitrary operators

[6] Split-step with more than these two bases is however possible in other schemes such as the finite element discrete variable representation [7]—each operator can be diagonalised and exponentiated locally in each element and applied as a (relatively small) matrix multiplication rather than using FFTs.

```
rev:     15 (206c9c70753a)
author:  Chris Billington <chrisjbillington@gmail.com>
date:    Sun Jul 24 16:55:15 2016 +1000
summary: Draft plots added to hidden variables section.

Blank page after contents page added.
```

and boundary conditions.

3.6.3 Results

Here I compare four numerical methods: Fourier split-step (FSS), fourth order Runge–Kutta in the interaction picture (RK4IP), ordinary fourth order Runge–Kutta (RK4), and my new method — fourth order Runge–Kutta in an instananeous local interaction picture (RK4ILIP).

The example chosen is a 2D simulation of a turbulent Bose–Einstein condensate, in both a rotating and nonrotating frame. For the nonrotating frame the differential equation simulated was equation (3.12), and for the rotating frame the same equation was with an additional two terms added to the Hamiltonian:

$$\hat{H}_{\text{rot}} + \hat{H}_{\text{comp}} = -\boldsymbol{\Omega} \cdot \hat{\boldsymbol{L}} + \frac{1}{2}\hbar m^2 \Omega^2 r^2 \tag{3.15}$$

$$= i\hbar\Omega\left(x\frac{\partial}{\partial y} - y\frac{\partial}{\partial x}\right) + \frac{1}{2}\hbar m^2 \Omega^2 r^2. \tag{3.16}$$

The addition of the first term transforms the original Hamiltonian into a frame rotating at angular frequency Ω in the (x, y) plane, and is equivalent to the the Coriolis and centrifugal forces that appear in rotating frames in classical mechanics [10]. The second term is a harmonic potential that exactly compensates for the centrifugal part of this force. In this way the only potential in the rotating frame is the applied trapping potential, and the only effect of the rotating frame is to add the Coriolis force.

Four trapping potentials were used, all radial power laws with different powers. These examples were chosen to demonstrate the specific situation in which RK4ILIP provides a benefit over the other methods for spatial Schrödinger-like equations, as discussed above.

The results of 120 simulation runs are shown in Figure 3.1. Each simulation was of a ^{87}Rb condensate in the $|F = 2, m_F = 2\rangle$ state, in which the two-body s-wave scattering length is $a = 98.98$ Bohr radii [11]. The simulation region was 20 μm in the x and y directions, and the Thomas–Fermi radius of the condensate was $R = 9$ μm. The chemical potential was $\mu = 2\pi\hbar \times 1.91$ kHz, which is equivalent to a maximum Thomas–Fermi density $\rho_{\text{max}} = 2.5 \times 10^{14}$ cm^{-3} and a healing length $\xi = 1.1$ μm. There were 256 simulation grid points in each spatial dimension, which is 14 points per healing length.

Four different potentials were used, all of the form $V(r) = \mu(r/R)^\alpha$ with $\alpha = 4, 8, 12, 16$. For the rotating frame simulations, the rotation frequency was $\Omega = 2\pi \times 148$ Hz. This is 89% of the effective harmonic trap frequency, defined as the frequency of a harmonic trap that would have the same Thomas–Fermi radius given the same chemical potential.

All ground states were determined using successive over-relaxation (See section [TODO]) with sixth-order finite differences for spatial derivatives. For the nonrotating simulations, convergence was reached with $\Delta\mu/\mu < 1 \times 10^{-13}$, with:

$$\Delta\mu = \sqrt{\frac{\langle\psi|(\hat{H} - \mu)^2|\psi\rangle}{\langle\psi|\psi\rangle}}, \tag{3.17}$$

where $\hat{H}$ is the nonlinear Hamiltonian and $\langle \boldsymbol{r}|\psi\rangle$ is the condensate wavefunction, which does not have unit norm. For the rotating frame simulations the ground states converged to $\Delta\mu/\mu \approx 9\times10^{-7}, 2\times10^{-6}, 3\times10^{-6}$ and 2×10^{-6} for $\alpha = 16, 12, 8$, and 4 respectively.

After each ground state was found, it was multiplied by a spatially varying phase factor corresponding to the phase pattern of a number of randomly positioned vortices:

$$\psi_{\text{vortices}}(x, y) = \psi_{\text{groundstate}}(x, y) \prod_{n=1}^{N} e^{\pm_n i \arctan 2(y-y_n, x-x_n)} \tag{3.18}$$

```
rev:     15 (206c9c70753a)
author:  Chris Billington <chrisjbillington@gmail.com>
date:    Sun Jul 24 16:55:15 2016 +1000
summary: Draft plots added to hidden variables section.

Blank page after contents page added.
```

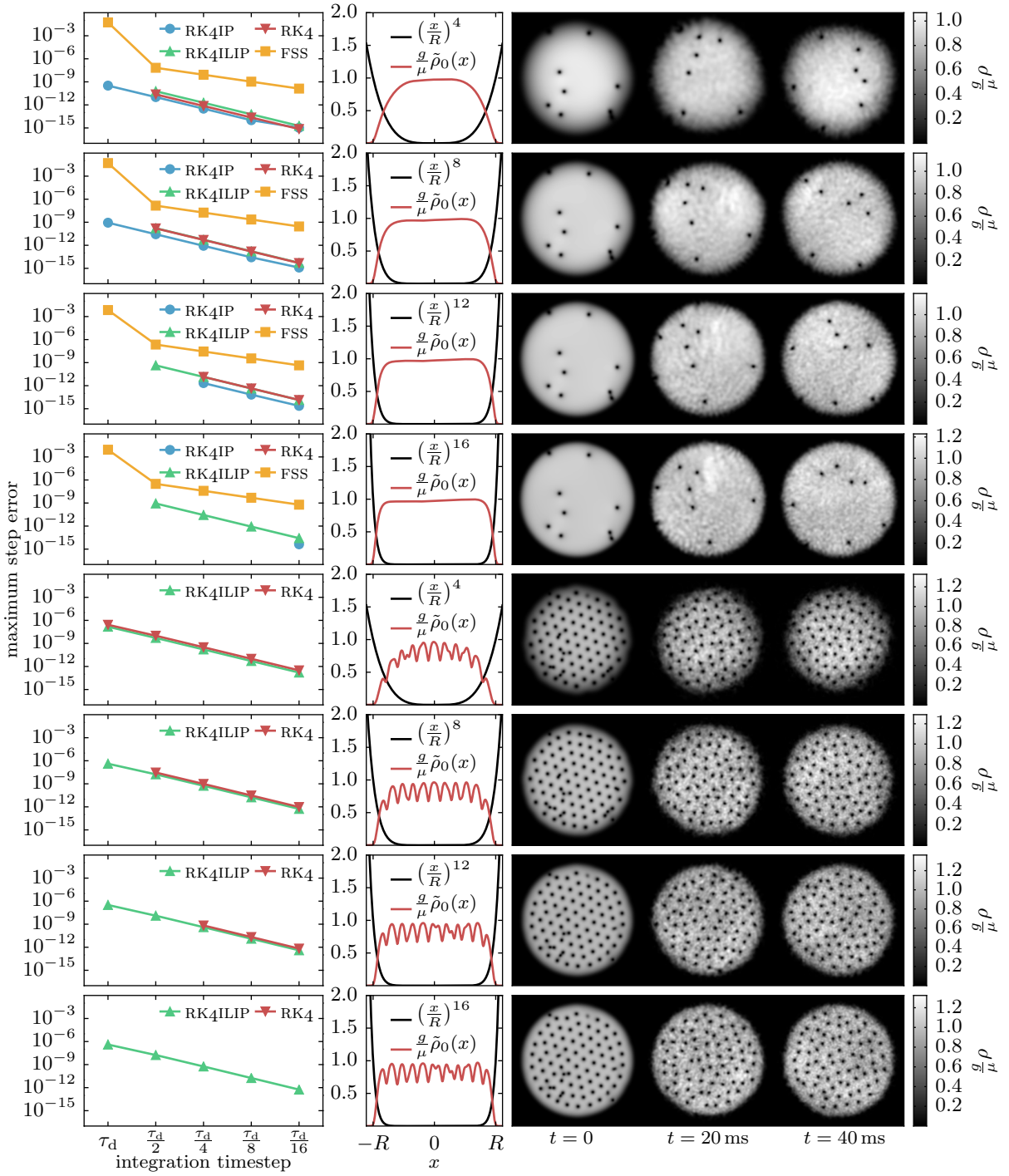

Figure 3.1: Results of simulations to compare RL4ILIP to other timestepping methods. Top four rows: Nonrotating frame simulations with four different radial power-law potentials. Bottom four rows: Rotating frame simulations with same four potentials. Left column: maximum per-step error $\int |\psi - \tilde{\psi}|^2 \,\mathrm{d}\boldsymbol{r} / \int |\tilde{\psi}|^2 \,\mathrm{d}\boldsymbol{r}$ of fourth order Runge–Kutta (RK4), its interaction picture variants (RK4IP and RK4ILIP) and Fourier split-step (FSS) as a function of timestep. Solutions were checked every 100 timesteps against a comparison solution $\tilde{\psi}$ computed using half sized steps for RK4 methods, and quarter sized steps for FSS. Simulations encountering numerical overflow not plotted. Centre column: potential (black) and average density $\tilde{\rho}_0$ of the initial state (red) over a slice of width $R/5$ in the y direction. Right column: Density of solution at initial, intermediate and final times for each configuration simulated (taken from RK4ILIP results). RK4ILIP is the only method usable in rotating frames and not encountering overflow in the steeper traps for the timesteps considered.

```
rev:     15 (206c9c70753a)
author:  Chris Billington <chrisjbillington@gmail.com>
date:    Sun Jul 24 16:55:15 2016 +1000
summary: Draft plots added to hidden variables section.

Blank page after contents page added.
```

where arctan2 is the two-argument arctan function,[7] $N = 30$, $\pm_n$ is a randomly chosen sign, and (x_n, y_n) are vortex positions randomly drawn from a Gaussian distribution centred on $(0, 0)$ with standard deviation equal to the Thomas–Fermi radius R. The same seed was used for the pseudorandom number generator in each simulation run, and so the vortex positions were identical in each simulation run.

[7] Defined as the principle value of the argument of the complex number $x + iy$: $\text{arctan2}(y, x) = \text{Arg}(x + iy)$.

After vortex phase imprinting, the wavefunctions were evolved in imaginary time [5]. For the nonrotating frame simulations, imaginary time evolution was performed for a time interval equal to the chemical potential timescale $\tau_\mu = 2\pi\hbar/\mu$, and for the rotating frame simulations, for $\tau_\mu/10$. This was done to smooth out the condensate density in the vicinity of vortices, producing the correct density profile for vortex cores. However, since imaginary time evolution decreases the energy of the state indiscriminately, it also had the side effect of causing vortices of opposite sign to move closer together and annihilate. This decreased the number of vortices, and is the reason the smoothing step in the rotating frame simulations was cut short to $\tau_\mu/10$, as otherwise all vortices had time to annihilate with one of the lattice vortices. A vortex pair in the process of annihilating is visible in Figure 3.1 as a partially filled hole in the initial density profile near the top of the condensate in the $\alpha = 4$, 12, and 16 rotating frame simulations.[8]

[8] The initial states for the four different potentials are not identical, so by chance the corresponding vortex in the $\alpha = 8$ case was not close enough to a lattice vortex to annihilate.

The smoothed, vortex imprinted states were then evolved in time for 40 ms. For each simulation, five different timesteps were used: $\Delta t = \tau_\text{d}, \tau_\text{d}/2, \tau_\text{d}/4, \tau_\text{d}/8, \tau_\text{d}/16$, where $\tau_\text{d} = m\Delta x^2/\pi\hbar \approx 2.68\,\mu\text{s}$ is the dispersion timescale associated with the grid spacing Δx, defined as the time taken to move one gridpoint at the phase velocity of the Nyquist mode.

For the nonrotating frame simulations, spatial derivatives for the RK4 and RK4ILIP methods were determined using the Fourier method [see section TODO]. This was to ensure a fair comparison with the other two methods, which necessarily use Fourier transforms to perform computations pertaining due to the kinetic term.

For the rotating frame simulations, sixth-order finite differences with zero boundary conditions were used instead for the kinetic terms of the RK4 and RK4ILIP methods, which were the only two methods used for those simulations (due to the other methods being incompatible with the angular momentum operator required for a rotating frame). This choice was fairly arbitrary, but did allow the condensate to be closer to the boundary than is otherwise possible with the periodic boundary conditions imposed by use of the Fourier method for spatial derivatives. This is because the rotating frame Hamiltonian is not periodic in space, and so its discontinuity at the boundary can be a problem if the wavefunction is not sufficiently small there.

As shown in Figure 3.1, all methods tested generally worked well until they didn't work at all, with the per-step error of RK4-based methods being either small and broadly the same as the other RK4-based methods, or growing rapidly to the point of numerical overflow (shown as missing datapoints). The break down of FSS was less dramatic, though it too had a clear jump in its per-step error for larger timesteps. Comparing methods therefore came down to mostly whether or not a simulation experienced numerical overflow during the time interval being simulated.

The main result was that RK4ILIP and FSS remained accurate over the widest range of timesteps and trap steepnesses, with RK4 and RK4IP requiring ever smaller timesteps in order to not overflow as the trap steepness increased.

For the rotating frame simulations, which were only amenable to the RK4 and RK4ILIP methods, the same pattern was observed, with RK4 only working at smaller timesteps as the trap steepness was increased, and ultimately diverging for all timesteps tested at the maximum trap steepness. By contrast, RK4ILIP remained accurate over the entire range of timesteps at the maximum trap steepness.

```
rev:     15 (206c9c70753a)
author:  Chris Billington <chrisjbillington@gmail.com>
date:    Sun Jul 24 16:55:15 2016 +1000
summary: Draft plots added to hidden variables section.

Blank page after contents page added.
```

3.6.4 Discussion

As mentioned, RK4ILIP is mostly useful for continuum quantum mechanics only when there are large spatial differences in the potential, which cannot give rise to equally large kinetic energies[9]. Furthermore, the advantage that RK4ILIP has over other methods with that same property is that it is does not require a particular form of Hamiltonian or a particular method of evaluating spatial derivatives. The former means is is applicable in rotating frames or to situations with unusual Hamiltonians, and the latter means is can be used with finite differences or FEDVR [7] and thus is amenable to parallelisation on a cluster computer.

[9] This is essentially due to such a situation violating the condition we laid out at the beginning of this section — that the simulation basis must be nearly an eigenbasis of the total Hamiltonian.

The ability to model large spatial variations in the potential provides only a narrow domain of increased usefulness over other methods. If a large kinetic energy results from the large potential, then the method requires just as small timesteps as any other. And if the large potential is supposed to approximate an an infinite well, then an actual infinite well may be modelled using zero boundary conditions, negating the need for something like RK4ILIP. However, when potential wells are steep, but not infinitely steep, here RK4ILIP provides a benefit. The only other model that can handle these large potentials—Fourier split-step—has the disadvantage that it cannot deal with arbitrary operators such as those arising from a rotating frame, and is not parallelisable with local data. The benefits of parallelisability are obvious, and the above results demonstrate RK4ILIP's advantage at simulating BECs in tight traps and rotating frames.

For systems with discrete degrees of freedom, RK4ILIP may be useful in the case where an approximate diagonalisation of the Hamiltonian is analytically known, and when the Hamiltonian's eigenvalues vary considerably in time (making a single interaction picture insufficient to factor out dynamical phases throughout the entire simulation). In this situation an analytic transformation into the diagonal basis can be performed at each timestep (or the differential equation analytically re-cast in that basis in the first place), and RK4ILIP can be used to factor out the time-varying dynamical phase evolution at each timestep. An example may be an atom with a magnetic moment in a time-varying magnetic field which varies over orders of magnitude. The transformation into the spin basis in the direction of the magnetic field can be analytically performed, and if the field varies by orders of magnitude, so do the eigenvalues of the Hamiltonian. Although the eigenvalues in this case and other similar cases can be computed analytically too, unless all time dependence of the Hamiltonian is known in advance of the simulation, it would be difficult to incorporate this into a re-casting of the differential equation in a time-dependent interaction picture. RK4ILIP may be useful in these cases to automate this process and evolve the system in the appropriate interaction picture at each timestep.

```
rev:     15 (206c9c70753a)
author:  Chris Billington <chrisjbillington@gmail.com>
date:    Sun Jul 24 16:55:15 2016 +1000
summary: Draft plots added to hidden variables section.

Blank page after contents page added.
```

This page intentionally left blank

Chapter 8

Hidden variables for semiclassical models with state-dependent forces

Define/describe what a hidden variable theory is, drawing heavily on Aaronson's [12] explanations. Give examples, argue why the Schrodinger theory is appealing.

Motivate with Stern-Gerlach experiment, and derive the method, show what sorts of problems it solves and where it disagrees with other models, provide simulation results. Limitations: no time dependent potentials, no 3D.

Possibly include speculation about these:

Maybe include a test to see whether it actually does work in 3D as-is, since we haven't actually checked, we just haven't been able to show on paper that current behavior is correct in 3D (also haven't shown it's incorrect).

Time dependent potentials could potentially be handled by approximating unitary as product of part due to spatial variation in H, and part due to time variation in H. compute transition probs for both such that a transition can be attributed to one or the other - only do velocity jumps to conserve potential if due to spatial motion, as time dependent potential can exchange energy with particle.

Matrix scaling for Schrodinger theory, discuss methods: Sinkhorn-Knopp, Lineal, and my one. Compare time complexity of algorithms so as to define the computational complexity of the hidden variables semiclassical method. Method is of course parallelisable on GPU or similar so is fast on parallel machines even if matrix scaling is slow.

Discuss how it would make sense for the systems to behave in the presence of collisions w.r.t collapse of state vectors.

8.1 Approximate Markovian decoherence rate for separating wavepackets

Positional separation of two different internal states of an atom leads to decoherence of those states, with a decoherence factor $r_{ij}(t)$ equal to the overlap of the spatial wavefunctions of the two components in question a time t after they began separating. Approximating both wavepackets as initially overlapping Gaussians of width σ, ignoring dispersion, and assuming they separate with constant relative acceleration a_{ij}, the decoherence factor is

```
rev:     15 (206c9c70753a)
author:  Chris Billington <chrisjbillington@gmail.com>
date:    Sun Jul 24 16:55:15 2016 +1000
summary: Draft plots added to hidden variables section.

Blank page after contents page added.
```

$$r_{ij}(t) = \langle \psi_i(t) | \psi_j(t) \rangle \tag{8.1}$$

$$= C \int_{-\infty}^{\infty} e^{-\frac{x^2}{4\sigma^2}} e^{-\frac{(x-x_{\text{rel}})^2}{4\sigma^2} + ik_{\text{rel}}x} \, \mathrm{d}x, \tag{8.2}$$

where

$$x_{\text{rel}}(t) = \frac{1}{2} a_{ij} t^2 \tag{8.3}$$

and

$$k_{\text{rel}}(t) = \frac{m}{\hbar} a_{ij} t \tag{8.4}$$

are the wavepackets' relative[1] position and wavenumber due to acceleration for a time t starting from zero relative velocity, and

[1] a_{ij}, x_{rel} and k_{rel} are the acceleration, position, and wavenumber of the j^{th} component with respect to the i^{th} component, that is, $a_{ij} = a_j - a_i$, etc.

$$C^{-1} = \int_{-\infty}^{\infty} e^{-\frac{x^2}{2\sigma^2}} \, \mathrm{d}x \tag{8.5}$$

is a normalisation constant [TODO CHECK IF NEEDS TO BE SQUARED]. Note that this expression holds for any number of dimensions—relative motion is only along one axis so the integrals in all other directions equal one.

Evaluating the Gaussian integral (8.2) gives the following expression for the decoherence factor $r_{ij}(t)$:

$$r_{ij}(t) = e^{-\left[\frac{1}{8\sigma^2} x_{\text{rel}}^2 + \frac{i}{2} x_{\text{rel}} k_{\text{rel}} + \frac{\sigma^2}{2} k_{\text{rel}}^2\right]}. \tag{8.6}$$

This is a decoherence *factor*; it is the factor by which the (i, j) off-diagonal of the reduced density matrix for the atom's internal state will be reduced at time t. The corresponding decoherence *rate* is given by the logarithmic derivative of (8.6):

$$\Gamma_{ij}(t) = -\frac{1}{r_{ij}(t)} \frac{\mathrm{d}}{\mathrm{d}t} r_{ij}(t). \tag{8.7}$$

The fact that (8.6) does not describe a constant decoherence rate (i.e., it does not have the functional form of exponential decay) means that the back-action on the atom's internal state caused by measurements of its motional state will be different depending on the interval of time between measurements.

For example, the logarithmic derivative of (8.6) approaches zero as t goes to zero. This means that in the limit of infinitely frequent measurements, no decoherence occurs at all in between measurements, and the motional state is reset after each measurement such that the wavepackets never separate at all. This is the quantum Zeno effect, and its appearance in models of open quantum systems is usually treated as a reminder that the assumption of infinitely frequent strong measurements is unphysical [CITE].

Since experimentally we are not measuring atoms' motional states so frequently, we ought to wait until the wavepackets are completely separated before performing a projective measurement. As in quantum optics models of open quantum systems, in which the measurement interval "should be large enough to allow the photons to get away from the atom" [CITE The Quantum Jump Approach and Quantum Trajectories Gerhard C. Hegerfeldt], ours should be large enough for the atomic states to get away from each other.

```
rev:     15 (206c9c70753a)
author:  Chris Billington <chrisjbillington@gmail.com>
date:    Sun Jul 24 16:55:15 2016 +1000
summary: Draft plots added to hidden variables section.

Blank page after contents page added.
```

If at large enough times, a decoherence rate is independent of time, that decoherence is called Markovian at that timescale. A Markovian environment is one that has no memory of the decoherence process—it "forgets" any information caused by past interaction with the system. Even though at short times, all decoherence rates in quantum mechanics tend to zero [CITE], if they become Markovian on a timescale shorter than other timescales of interest, the Markov approximation can be used and a constant decoherence rate used at all times. In quantum optics, the decoherence factor for the internal state of an atom due to photon emission indeed tends to exponential decay on timescales that are still much shorter than that of the system evolution, and thus the Markov approximation is accurate.

Unlike quantum optics models, our decoherence factor does not describe Markovian decoherence on any timescale. In the limit of large t, its functional form is e^{-t^4}, not the exponential decay required to treat the decoherence as Markovian [CITE] at that timescale. Nonetheless, if we wish to write a time-local differential equation for the internal state of the atom, Markovian decoherence is the only kind we can include [CITE].

To that end, we will now construct a "time ignorant" version of $r_{ij}(t)$ that answers the question "What is the expected decoherence factor at all future times, if you don't know how long it has been since the two wavepackets began separating?" In this way we can compute an *average* decoherence rate Γ_{ij} described by our decoherence factor, even though $r_{ij}(t)$ does not have a constant decoherence rate at large times. This essentially amounts to finding the best fitting exponential to $r_{ij}(t)$. Whilst this approximation is crude, it is nonetheless an improvement over the Ehrenfest model, which has no decoherence at all (i.e. it has a decoherence rate that is also constant like ours—but equal to zero).

We define the time-ignorant decoherence factor $\tilde{r}_{ij}(t)$ as the overlap of the wavefunction of the i^{th} internal state with a superposition of wavepackets of the j^{th} internal state, with the superposition being over all times in the past the wavepackets began separating:

$$\tilde{r}_{ij}(t) = \langle\psi_i(t)| A \int_{-\infty}^{0} |\psi_j(t-t')\rangle \, \mathrm{d}t', \tag{8.8}$$

where A is a normalisation constant such that $\tilde{r}_{ij}(0) = 1$. Since $|\psi_i(t)\rangle$ is time independent (rather, since we can perform our calculations in the frame of reference in which it is stationary), this is:

$$\tilde{r}_{ij}(t) = A \int_{-\infty}^{0} r_{ij}(t-t') \, \mathrm{d}t', \tag{8.9}$$

which is simply the convolution of our decoherence factor with a step function which is nonzero at all negative times. Our average decoherence rate Γ_{ij} is then given by the logarithmic derivative of $\tilde{r}_{ij}(t)$ at $t = 0$:

$$\Gamma_{ij} = -\frac{\tilde{r}'_{ij}(0)}{\tilde{r}_{ij}(0)} \tag{8.10}$$

$$= -\frac{\int_0^\infty \tilde{r}'_{ij}(t) \, \mathrm{d}t}{\int_0^\infty \tilde{r}_{ij}(t) \, \mathrm{d}t} \tag{8.11}$$

$$\Rightarrow \Gamma_{ij}^{-1} = \int_0^\infty e^{-\left[\frac{1}{8\sigma^2} x_{\text{rel}}^2 + \frac{i}{2} x_{\text{rel}} k_{\text{rel}} + \frac{\sigma^2}{2} k_{\text{rel}}^2\right]} \mathrm{d}t. \tag{8.12}$$

As mentioned, Γ_{ij} is the decay constant for the best fitting exponential to our decoherence factor (8.6). Although (8.6) looks nothing like a decaying exponential in time, an exponential approximation to it nonetheless ought to decay to zero on the same timescale. An example of this is shown in Figure 8.1

```
rev:     15 (206c9c70753a)
author:  Chris Billington <chrisjbillington@gmail.com>
date:    Sun Jul 24 16:55:15 2016 +1000
summary: Draft plots added to hidden variables section.

Blank page after contents page added.
```

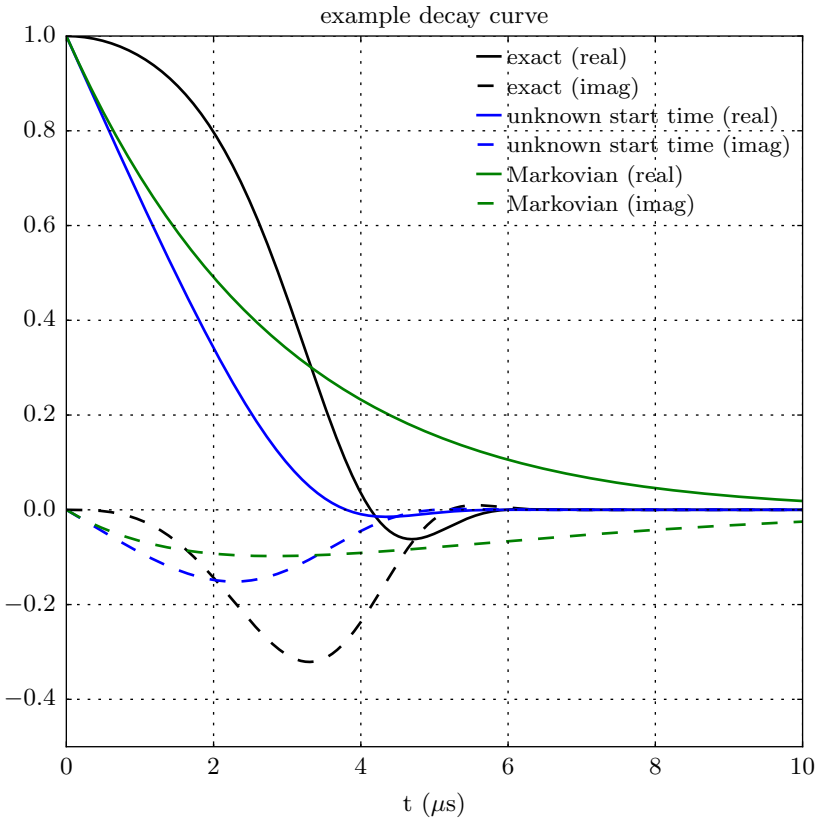

Figure 8.1: Caption.

In order to obtain an approximate analytic expression for this integral, we consider two limiting cases and then stitch them together in the intermediate regime. In the limit of small wavepackets, σ is small and thus the first term in the exponent in (8.12) is largest, and the third term is smallest. In this regime, which describes when positional separation (as opposed to separation in k-space) dominates the decoherence, we'll neglect the third term in the exponent and treat the second term as small relative to the first. This gives us:

$$\Gamma^{-1}_{ij\,(\mathrm{pos})} \approx \int_0^\infty e^{-\left[\frac{1}{8\sigma^2}x_{\mathrm{rel}}^2 + \frac{i}{2}x_{\mathrm{rel}}k_{\mathrm{rel}}\right]}\,\mathrm{d}t. \tag{8.13}$$

$$\approx \int_0^\infty e^{-\frac{1}{8\sigma^2}x_{\mathrm{rel}}^2}\left(1 - \frac{i}{2}x_{\mathrm{rel}}k_{\mathrm{rel}}\right)\,\mathrm{d}t. \tag{8.14}$$

$$= 2^{\frac{5}{4}}\Gamma(\tfrac{5}{4})\sqrt{\frac{\sigma}{a_{ij}}} - 2i\frac{m\sigma^2}{\hbar}, \tag{8.15}$$

where we used a first-order Taylor expansion of an exponential in (8.14). We similarly use a first order expansion to take the reciprocal of (8.15) (since the second term is much smaller than the first[2]), and arrive at:

$$\Gamma_{ij\,(\mathrm{pos})} \approx \frac{1}{2^{\frac{5}{4}}\Gamma(\frac{5}{4})}\sqrt{\frac{a_{ij}}{\sigma}} + \frac{i}{2\sqrt{2}\Gamma(\frac{5}{4})^2}\frac{m\sigma a_{ij}}{\hbar} \tag{8.16}$$

[2] This isn't necessary in order to obtain a simple expression for $\Gamma_{ij\,(\mathrm{pos})}$—the reciprocal without this approximation is equally simple—but it leaves us with power laws for the real and imaginary parts of $\Gamma_{ij\,(\mathrm{pos})}$, which are easier to stitch together with those from the large σ regime.

```
rev:     15 (206c9c70753a)
author:  Chris Billington <chrisjbillington@gmail.com>
date:    Sun Jul 24 16:55:15 2016 +1000
summary: Draft plots added to hidden variables section.

Blank page after contents page added.
```

Similarly for the large σ regime, we neglect the first term in the exponent of (8.12) and consider the second term small relative to the third. This is the regime in which the decrease in overlap of the two wavepackets is dominated by their separation in velocity space. Following the same process as above gives:

$$\Gamma^{-1}_{ij\,(\mathrm{vel})} \approx \int_0^\infty e^{-\left[\frac{i}{2}x_{\mathrm{rel}}k_{\mathrm{rel}}+\frac{\sigma^2}{2}k^2_{\mathrm{rel}}\right]}\,\mathrm{d}t. \tag{8.17}$$

$$\approx \int_0^\infty \left(1-\frac{i}{2}x_{\mathrm{rel}}k_{\mathrm{rel}}\right)e^{-\frac{\sigma^2}{2}k^2_{\mathrm{rel}}}\,\mathrm{d}t \tag{8.18}$$

$$= \sqrt{\frac{\pi}{2}}\frac{\hbar}{m\sigma a_{ij}} - i\frac{\hbar^3}{2m^3\sigma^4 a_{ij}^2} \tag{8.19}$$

$$\Rightarrow \Gamma_{ij\,(\mathrm{vel})} \approx \sqrt{\frac{2}{\pi}}\frac{m\sigma a_{ij}}{\hbar} + \frac{i}{\pi}\frac{\hbar}{m\sigma^2} \tag{8.20}$$

Equations (8.16) and (8.20) are our final expressions for the docoherence rate in the limit of small and large wavepackets respectively. Adding their real parts in quadrature and adding the reciprocals of their imaginary parts then provides a reasonable approximation for Γ_{ij} over all wavepacket sizes:

$$\Gamma_{ij} \approx \left[\mathrm{Re}(\Gamma_{ij\,(\mathrm{pos})})^2 + \mathrm{Re}(\Gamma_{ij\,(\mathrm{vel})})^2\right]^{\frac{1}{2}} + i\left[\mathrm{Im}(\Gamma_{ij\,(\mathrm{pos})})^{-1} + \mathrm{Im}(\Gamma_{ij\,(\mathrm{vel})})^{-1}\right]^{-1}. \tag{8.21}$$

We now have an approximate analytic expression that not computationally inexpensive to evaluate for each atom in an ensemble at every timestep of a differential equation. An example showing the accuracy of (8.21), compared to the exact expression (8.12) for for Γ_{ij} over a range of wavepacket sizes is shown in Figure 8.2.

8.2 Choice of wavepacket size

How big is a wavepacket?

```
rev:     15 (206c9c70753a)
author:  Chris Billington <chrisjbillington@gmail.com>
date:    Sun Jul 24 16:55:15 2016 +1000
summary: Draft plots added to hidden variables section.

Blank page after contents page added.
```

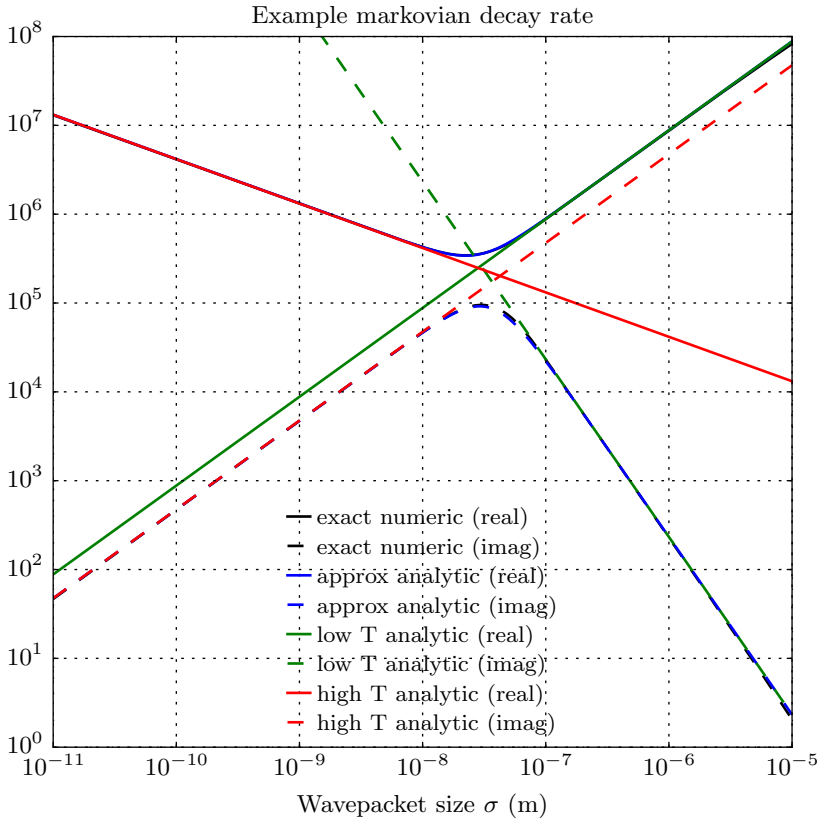

Figure 8.2: Caption.

```
rev:     15 (206c9c70753a)
author:  Chris Billington <chrisjbillington@gmail.com>
date:    Sun Jul 24 16:55:15 2016 +1000
summary: Draft plots added to hidden variables section.

Blank page after contents page added.
```

References

[1] J. J. Sakurai. *Modern quantum mechanics*. Addison-Wesley Pub. Co, Reading, Mass (1994). [p 3]

[2] Benjamin M. Caradoc Davies. *Vortex dynamics in Bose–Einstein condensates*. PhD thesis, University of Otago, Dunedin, New Zealand (2000). [p 4]

[3] W.H. Press. *The art of scientific computing*. Cambridge University Press (1992). [p 5]

[4] C.J. Pethick and H. Smith. *Bose–Einstein condensation in dilute gases*. Cambridge University Press (2002). [p 5]

[5] M. L. Chiofalo, S. Succi, and M. P. Tosi. *Ground state of trapped interacting Bose–Einstein condensates by an explicit imaginary-time algorithm*. Phys. Rev. E **62**, 7438 (2000). DOI: 10.1103/PhysRevE.62.7438. [pp 6 and 10]

[6] G.M. Muslu and H.A. Erbay. *Higher-order split-step Fourier schemes for the generalized nonlinear Schrödinger equation*. Mathematics and Computers in Simulation **7**, 581 (2005). DOI: 10.1016/j.matcom.2004.08.002. [p 7]

[7] Barry I. Schneider, Lee A. Collins, and S. X. Hu. *Parallel solver for the time-dependent linear and nonlinear schrödinger equation*. Phys. Rev. E **73**, 036708 (2006). DOI: 10.1103/PhysRevE.73.036708. [pp 7 and 11]

[8] M.A. Heroux, P. Raghavan, and H.D. Simon. *Parallel processing for scientific computing*. Society for Industrial and Applied Mathematics, Philadelphia, PA (2006). [p 7]

[9] Anshul Gupta and Vipin Kumar. *The scalability of FFT on parallel computers*. IEEE Transactions on Parallel and Distributed Systems **4**, 922 (1993). [p 7]

[10] P. Gulshani and D. J. Rowe. *Quantum mechanics in rotating frames. i. the impossibility of rigid flow*. Canadian Journal of Physics **56**, 468 (1978). DOI: 10.1139/p78-060. [p 8]

[11] E. G. M. van Kempen, S. J. J. M. F. Kokkelmans, D. J. Heinzen, and B. J. Verhaar. *Interisotope determination of ultracold rubidium interactions from three high-precision experiments*. Phys. Rev. Lett. **88**, 093201 (2002). DOI: 10.1103/PhysRevLett.88.093201. [p 8]

[12] Scott Aaronson. *Quantum computing and hidden variables*. Phys. Rev. A **71**, 032325 (2005). DOI: 10.1103/PhysRevA.71.032325. [p 13]


```
rev:     15 (206c9c70753a)
author:  Chris Billington <chrisjbillington@gmail.com>
date:    Sun Jul 24 16:55:15 2016 +1000
summary: Draft plots added to hidden variables section.

Blank page after contents page added.
```